First-principles study of the $TiO_2(110)$ surface reduction upon Na adsorption

Tristan Albaret,* Fabio Finocchi, and Claudine Noguera
Laboratoire de Physique des Solides, UMR-CNRS 8502 Bâtiment 510, Université Paris Sud, 91405 Orsay, France

Alessandro De Vita
Institut Romand de Recherche Numérique en Physique des Matériaux (IRRMA), PPH-Ecublens, CH-1015 Switzerland and INFM and Dipartimento di Ingegneria dei Materiali, Università di Trieste, via A. Valerio 2, 34127 Trieste, Italy
(Received 26 April 2001; published 14 December 2001)

We present a detailed theoretical study, based on density-functional calculations, of Na adsorption on $TiO_2(110)$ for coverage equal to 1/8, 1/4, and 1/2 monolayers. Two competing threefold adsorption sites are found. In the framework of the Bader theory, we analyze the electron distribution, the interfacial electron transfer, and the screening processes as a function of the coverage and the actual adsorption geometry. At low coverage, the Na atoms bind preferentially to two bridging and one in-plane O atoms. The adsorbed sodium atoms are nearly fully ionized. The excess electron states have a nonbonding Ti character and are delocalized over a few surface and subsurface sites. Such a behavior, which is at variance with the common belief that the excess states should be essentially localized on the surface fivefold titanium, is discussed in terms of the surface electrostatic potential and the atomic relaxations. According to our calculations, the onset of covalent interactions between Na atoms occurs for coverage slightly below 1/2 of monolayer, depending on the specific adsorption configuration. It is accompanied by a reduction of the positive Bader charge of the Na atoms and by a weakening of the ionic Na-O bond strength, which results in decreasing Na adsorption energies. At 1/2 monolayer coverage, the adsorption energies are practically insensitive to the details of the Na distribution among the low-energy adsorption sites, which suggests that Na-induced surface reconstructions might be affected by the intrinsic quality of the surface and the actual deposition conditions.

DOI: 10.1103/PhysRevB.65.035402 PACS number(s): 73.20.At, 73.20.Jc, 71.15.Nc, 68.43.−h

I. INTRODUCTION

Titanium-oxide surfaces are among the most studied systems in the field of surface physicochemistry, mainly because of the wide range of applications they may be used for. The photoelectrolysis properties of TiO_2 were first described in 1972 by Fujishima and Honda.[1] More generally, TiO_2 is known as a photocatalyst material that can be used for applications in environmental or biological sciences.[2,3] Its surfaces play a key role in several applications, such as gas sensor, waveguides, solar cells, and biocompatible implants. The preparation of the $TiO_2(110)$ rutile surface is nowadays a well-controlled process.[4] By tuning temperature and oxygen pressure, either stoichiometric or defective surfaces can be obtained reproducibly. Since reduced TiO_2 permits electronic conduction, scanning tunnelling microscopy experiments can be performed on TiO_2 surfaces, yielding local structural information on surface defects and/or adsorbates.[5] For these reasons, besides their technological interest, TiO_2 surfaces represent a model system to study the fundamental properties of oxide surfaces, and their interfaces with metal deposits.

Metal atoms deposited on oxide surfaces are known to modify the surface reactivity, which has important applications in heterogeneous catalysis. Metal-oxide interfaces, on the other hand, are met in various electronic devices, in electric contacts, when one wishes to confine liquid metals, etc. Many studies have been devoted to the deposition of transition and noble metals, on, e.g., $TiO_2(110)$ surfaces.[6,7] As regards alkali atoms, their strong electropositive character induces specific features in the interface formation and electronic structure, which are far from being fully elucidated. More specifically, in this paper, we will consider Na deposits on $TiO_2(110)$ and we will focus on the change, from ionic to metallic, in the adsorbate layer that takes place at increasing coverage. Furthermore, we will address the question of the strength of the electron transfer and its localization in the substrate.

X-ray photoemission (XPS) measurements on Cs/TiO_2,[8,9] K/TiO_2,[10,11] and Na/TiO_2,[12,13] reveal a characteristic peak at low binding energy in the Ti core level spectrum and the existence of states in the band gap of the oxide. The XPS peak is also observed on oxygen-defective surfaces[14] and on UV-irradiated surfaces,[15] suggesting some similarity between the electronic structure of defective and alkali-covered surfaces. Up to approximately one monolayer (ML), these results support a model in which the alkali atoms are nearly fully ionized, form ionic bonds with the substrate and induce a reduction of surface Ti^{4+} ions into Ti^{3+} species. Interestingly, upon Na adsorption, a (4×2) surface reconstruction has been evidenced at $c=1/2$ ML,[12] which was assigned to the formation of Na_2O surface entities. At higher coverage, metallic bonds start to form between adsorbates, and the growth mode changes from two-dimensional (2D) to three-dimensional (3D). This simple picture is supported by D^+ scattering mesurements[16] that are sensitive to the net charge of the surface alkali atoms. Relevant to changes in the electronic structure, it has been shown[12,13] that the presence of Na on TiO_2 (110) induces the formation of carbonates when the surface is exposed to CO_2, although no such reaction occurs on the clean stoichiometric surface.

From a theoretical point of view, in the low-coverage re-

gime, adsorption sites and charge transfer have been determined for $K/TiO_2(100)$ by an *ab initio* periodic density functional (DFT) method,[17] and for $K/TiO_2(110)$ by periodic Hartree-Fock (HF),[18,19] and embedded cluster HF calculations.[18] $Na/TiO_2(110)$ has been studied with embedded cluster calculations beyond HF,[20,21] molecular dynamics using empirical interatomic potentials[21] and periodic HF calculations.[22]

The theoretical results are in general agreement with the experiments, predicting a large electron transfer from the alkali to the surface and ionic bonding, but they provide no detailed understanding of the electronic-charge redistribution at the metal-oxide interface. As regards the evolution of the interfacial electronic structure as a function of coverage, although it was recognized in the case of $K/TiO_2(110)$ that the ionic character of the interfacial bond can be strongly altered, especially for geometries that favor attractive adsorbate-adsorbate interactions,[18] it is still unclear under which circumstances such interactions can overcome the strong electrostatic repulsion between alike cations that is present at low coverage.

In this work, we present a detailed theoretical study of Na adsorption on $TiO_2(110)$ based on DFT/L(S)DA [local (spin) density approximation] *ab initio* calculations. Electronic degrees of freedom and atomic positions are fully optimized for different surface configurations and for various coverage. Following Bader's topological model,[23,24] we analyze in details the electron redistributions and the screening of Na^+ ions as a function of coverage. In order to better elucidate the adsorption mechanism, we discuss the relative strength of the adsorbate-surface and adsorbate-adsorbate interactions, and the interpretation of photoemission experiments.

The paper is organized as follows. Section II describes our computational method, the charge analysis technique, and the slab geometries used. In Sec. III and Sec. IV, we present and discuss the energetics, adsorption geometry, electronic structure, and charge analysis for Na deposition at low ($c=1/8$ ML) and higher ($c=1/4$ and 1/2 ML) coverage, respectively. Section V focuses on Na-Na interactions at $c=1/2$ ML.

II. COMPUTATIONAL METHOD

We perform *ab initio* calculations within the framework of DFT[25,26] to achieve a self-consistent electronic structure and geometry optimization. The Kohn-Sham states and the electronic density are expanded on a plane-wave basis set. exchange and correlation effects are treated within the LDA or LSDA using the Perdew-Zunger parametrization.[27] We use norm-conserving soft pseudopotentials of Trouiller and Martins[28] in the Kleinman-Bylander form[29] to represent the interaction between valence electrons and the ionic cores. For oxygen, $2s$ and $2p$ electrons are treated explicitly in the valence. For titanium, it has been shown[30,31] that semi-core states participate to the Ti-O bonds and, therefore, we explicitly include $3s$, $3p$, and $3d$ electrons in the self-consistent electron distribution. Local components for oxygen and titanium are *d* and *s*, respectively.

As for titanium, the influence of semi-core states polarization was checked to construct the sodium pseudopotential. For this purpose we performed structural tests on the linear Na_2O molecule with two distinct pseudopotentials. The first one ($\hat{V}_a$) only includes Na $3s$ electrons as valence electrons and has a *p* local component, while the second pseudopotential ($\hat{V}_b$) explicitly includes Na $2s$, $2p$, and $3s$ electrons in the valence with the *s* taken as the local component. The calculated bond lengths (3.74 a.u. for $\hat{V}_a$ and 3.70 a.u. for $\hat{V}_b$) can be compared with the accurate value of 3.83 a.u. obtained by means of all-electron DFT-GGA calculation.[32] Thus, allowing the Na semi-core electrons to relax little influences the Na-O bond, with respect to other approximations such as the choice of the exchange and correlation energy functional. Accordingly, we adopt ($\hat{V}_a$) in all surface calculations. We use a plane-wave cut-off energy of 60 Ry, which gives accurate results for small molecules TiO and TiO_2.[33]

We perform a quantitative analysis of the electron density following the prescriptions of Bader's theory of atoms in molecules.[23,24] According to Bader, in a condensed phase, each atom *i* can be assigned a space region V_i, which contains a maximum of the total electron density $\rho(\vec{r})$ and is enclosed within a surface determined by the zero-flux condition: $\vec{\nabla}\rho\cdot\vec{n}=0$ ($\vec{n}$ the vector orthogonal to the surface). The integration of $\rho(\vec{r})$ within the volumes V_i yields the total electron numbers N_i and thus the ionic charges Q_i. In the limit of full convergence for the electronic-structure calculation, Bader charges are independent of the basis set used for the expansion of the electronic wave functions, at variance with charges derived from a Mulliken population analysis. In the case of covalent and very diffuse orbital hybridization, additional maxima of the electronic density may exist on some bonds. They are usually referred to as ''pseudoatoms'' or ''nonnuclear attractors'' and they are also enclosed within zero-flux surfaces.

Following Bader's scheme, we perform a numerical integration of $\rho(\vec{r})$ in three steps. First, $\rho(\vec{r})$ is represented on a real space cubic grid of stride δa. Then the maxima of $\rho(\vec{r})$ are found. In the last step, $\rho(\vec{r})$ is integrated in each basin, starting from the maximum and following paths between neighboring grid points bearing decreasing densities. In doing so, regions containing the interatomic surfaces are shared between different atomic basins. To enforce charge conservation, we equally distribute the electron density of these regions among the neighboring basins. The accuracy of this scheme can be systematically improved by decreasing the grid parameter δa. In practice, we use $\delta a=0.1$ a.u., which gives an estimated maximum error on the ionic charges smaller than 0.1 electron. A similar charge analysis was performed and validated in an earlier study of unsupported Ti_nO_m clusters.[30]

We model the rutile $TiO_2(110)$ surface by slabs made of *n* repeat units of O/2(TiO)/O composition, as shown in Fig. 1, with $n=3$ or $n=5$. The $n=3$ ($n=5$) slabs are separated by a vacuum layer 10 (15) a.u. thick, respectively. A 2D (2×2) supercell is used in the calculations. The cell dimen-

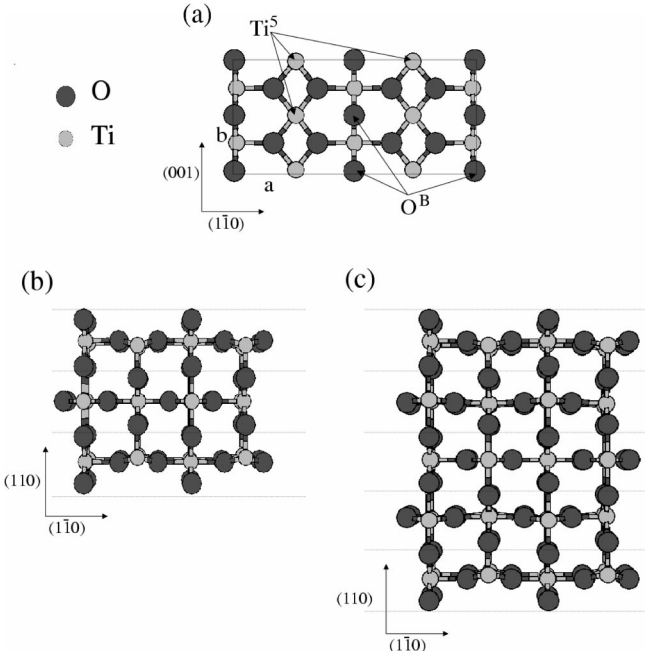

FIG. 1. Geometry used for modeling the TiO_2 (110) surface: (a): view of the topmost plane of the 2D (2×2) supercell. The positions of the undercoordinated atoms, the fivefold titaniums Ti^5, and the twofold bridging oxygens O^B, are indicated. (b) and (c): (001) views of the $n=3$ and $n=5$ slabs, respectively. The horizontal dashed lines indicate the average interlayer positions.

sions $a=24.35$ a.u., and $b=11.07$ a.u. are taken from a separate bulk calculation.[30] Only the Γ point is used for Brillouin zone integration. With this setup, the clean surface energy is equal to 0.89 J/m^2 (0.66 J/m^2) for $n=3$ ($n=5$), respectively. It compares within roughly 20% with a previous DFT-LDA calculation performed with a finer $\vec{k}$-point sampling.[34] The surface relaxations, on the other hand, are reproduced with an accuracy better than 0.04 a.u.

Na atoms are adsorbed in equal number on each face of the slab, and, in agreement with previous conventions used in the literature, we define the coverage c as half their number per (1×1) 2D unit cell (for example, $c=1/2$ ML corresponds to four Na atoms per supercell on each side of the slab). The equilibrium geometries are obtained by applying a damped dynamic algorithm until the forces on each atom are less than 15 meV/a.u. The starting configurations for the sodium are chosen without imposing any particular symmetry. Our largest production calculations are performed within the LSDA for $c=1/8$, with an $n=5$ slab. For higher coverage, $n=3$ slabs and the LDA are used with a constrained state occupancy.

III. ADSORPTION AT $C=1/8$ ML

In this section, we present and discuss the characteristics of Na adsorption for the lowest coverage allowed by our choice of the 2D supercell, i.e., $c=1/8$ ML. Comparison with higher coverage (see Sec. IV) shows that Na-Na interactions are weak at this coverage. Most of the adsorption characteristics discussed here are thus representative of isolated adsorbed Na atoms.

A. Adsorption geometries and energetics

Initial adsorption configurations were chosen in such a way that the largest number of Na-O bonds are formed, i.e., three in the case of $TiO_2(110)$. The two most stable optimized geometries are depicted in Fig. 2. In the first one (which we refer to as the *A* configuration in the following) Na is bound to two bridging (O^B) and one in-plane (O^P) oxygen atoms. In the *B* configuration, Na is adjacent to one O^B and two O^P. In both cases, the Na coordination number Z_{Na} is equal to 3. These configurations were also found to have a low energy in other theoretical studies of Na[21] and K[18] adsorption on $TiO_2(110)$.

Fully relaxed interatomic distances and adsorption energies are reported in Table I and compared with other theo-

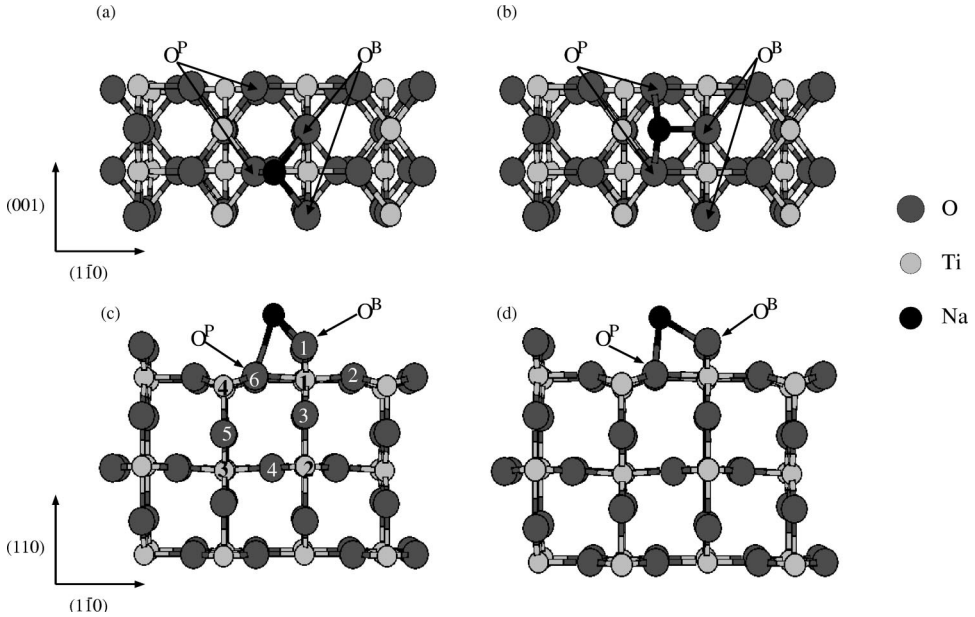

FIG. 2. Adsorption geometries at $c=1/8$ ML. Views along (001) and (110) directions: (a) and (c): *A* configuration; (b) and (d): *B* configuration. In (c) and (d) only the upper half of the slabs is represented.

TABLE I. Adsorption energies and adsorption geometries obtained in the present work (left panels), compared to bond energies and bond lengths found in other Na-O compounds (right panels).

Adsorption energies (eV) $Na/TiO_2(110)$				Energy/Bond (eV) Other Na-O compounds		
	Z_{Na}	Present work	Other theory [a]		Z_{Na}	E/bond
A site	3	2.42		Na_2O (molecule)	1	2.71, [b] 2.56 [c]
	2		7.11	Na_2O (bulk)	4	1.12, [b] 1.14 [d]
B site	3	2.18				

Na-O bond lengths (a.u.) $Na/TiO_2(110)$				Na-O bond lengths (a.u.) Other Na-O compounds		
		Present work	Other theory [a]		Z_{Na}	d(Na-O)
		($Z_{Na}=3$)	($Z_{Na}=2$)	Na_2O (molecule)	1	3.74 [b]
A site	d(Na-O^B)	4.25	4.46	Na_2O (bulk)	4	4.56, [b] 4.55 [d]
	d(Na-O^P)	4.53	6.39	$Na_2Ti_4O_9$ (bulk)	6	4.65 [e]
B site	d(Na-O^B)	3.95		$Na_2Ti_4O_9$ (bulk)	8	4.89 [e]
	d(Na-O^P)	4.85				

[a]Embedded cluster calculations Ref. 20.
[b]Calculation performed with our numerical setting.
[c]Experiment Ref. 35.
[d]Experiment Ref. 36.
[e]Experiment Ref. 37.

retical and experimental results.

As regards Na-O bond lengths, we note that, in both configurations, the Na-O^P distance is larger than the Na-O^B one. However, the highest value ($d_{Na-O^P}=4.85$ a.u. for B sites) lies in the range of Na-O bond lengths in $Na_2Ti_4O_9$ bronzes (see Table I, right panel). No bond disruption thus occurs,[38] at variance with the results of Ref. 20 ($d_{Na-O^P}=6.39$ a.u.), in which the Na coordination number Z_{Na} lies closer to 2 than to 3. The Na-O bond-lengths recorded in the right part of Table I in various Na-O compounds follow the general trend that interatomic distances increase as the coordination numbers of the partner atoms get larger.[39] Our calculated interatomic distances for adsorbed Na on TiO_2 fit the general trend, considering the local environment of the adsorbed Na ($Z_{Na}=3$) and the fact that the in-plane oxygens have a larger coordination number than the bridging oxygen atoms ($Z_{O^B}=2$ versus $Z_{O^P}=3$).

In the substrate, adsorption induces nonnegligible relaxations, which mainly involve Ti-O bonds in the vicinity of Na. The most noticeable ones take place along the [110] direction, with a succession of bond elongations and contractions below the bridging oxygens and the Na site (e.g., +0.10 a.u., −0.14 a.u., +0.11 a.u., for the O_1Ti_1, Ti_1O_3, and O_3Ti_2 distances, with the atom labels indicated in Fig. 2 for the A geometry). Their signs are opposite to those of the clean-surface displacements, thus revealing a partial surface derelaxation consequent to the Na adsorption. This result is consistent with the interpretation given in Ref. 40 for the disappearance of a resonant photoemission feature of the clean surface upon Na adsorption.

We find the adsorption A site to be more stable than the B site, by 0.24 eV. Such an energy difference, although small, is significant since it is much larger than our estimated numerical error. While the Na coordination number is equal in both cases ($Z_{Na}=3$), the A configuration maximizes the number of Na bonds with bridging oxygens. This result is consistent with the general trend that total cohesive energies increase with the coordination numbers Z of the partner atoms less quickly than Z.[39] The bond energy is thus larger when the coordination Z of the partner atoms is smaller, as exemplified in the right part of Table I for the Na_2O molecule ($Z_{Na}=1, Z_O=2$) and bulk antifluorite phase ($Z_{Na}=4, Z_O=8$). Here, the trend also applies since $Z_{O^B}=2$ and $Z_{O^P}=3$.

B. Electronic structure

The electronic structures of the A and B configurations are very similar, and we shall only discuss the former. The density of states (DOS) in the valence band (VB) and the Ti_{3s} and Ti_{3p} energy ranges is shown in Fig. 3 and compared to that of the clean surface. A noticeable feature is the existence of an occupied state in the gap of the clean surface, located 1.77 eV above the VB maximum (1.75 eV for the B configuration), which is nearly fully spin-polarized. This state is associated to the increase of the total number of valence electrons upon adsorption (one additional electron per adsorbed sodium), and will be referred to in the following as an ''excess electronic state.'' This gap state was observed in photoemission spectra at $\simeq +2.9$ eV Refs. 12,13 and was found in other theoretical works on Na/TiO_2 (110) (at +2.35 eV Ref. 22) and $K/TiO_2(110)$ (at +2.0 eV Ref. 18).

The nature of the excess states is clarified by direct visualization of the spin density that is represented in Fig. 4. The

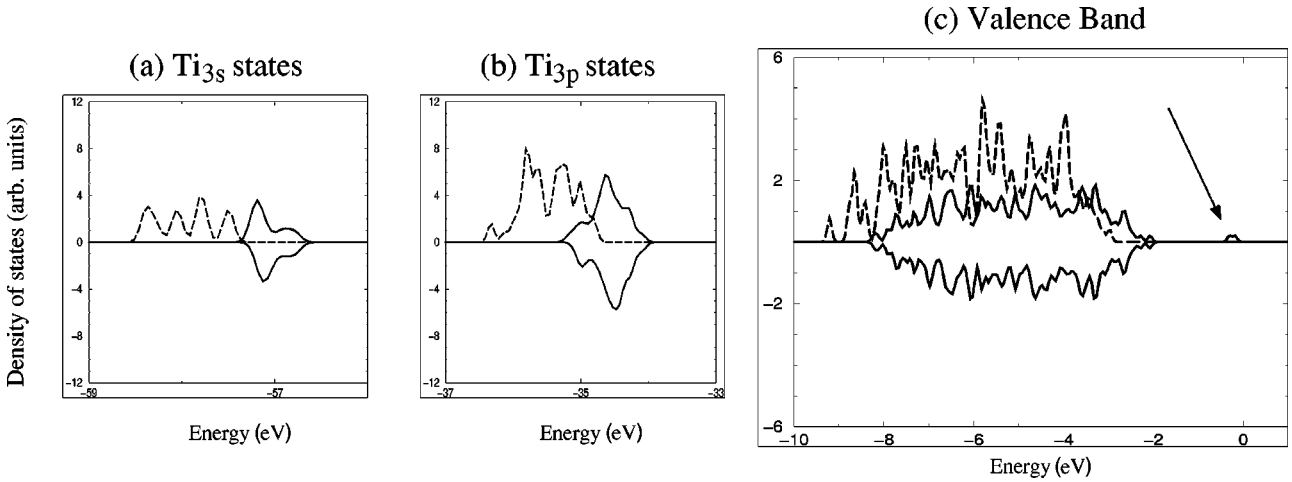

FIG. 3. $Na/TiO_2(110)$ DOS (arbitrary units) as a function of energy (in eV), at $c=1/8$ ML, in (a) the Ti_{3s}, (b) the Ti_{3p}, and (c) the VB energy windows. Solid lines: $Na/TiO_2(110)$. Dashed lines: clean $TiO_2(110)$ surface. DOS of spin-up (spin-down) states are in positive (negative) arbitrary units. The arrow points the position of the excess electronic state of the $Na/TiO_2(110)$ surface.

isodensity map shows that the excess state is essentially localized on substrate titaniums, with a dominant weight on those lying in the subsurface plane just below the surface fivefold coordinated titaniums. Nearly no weight is found on the adsorbed Na, nor on the substrate oxygens. This characteristic gives support to the existence of a large electron transfer from the adsorbate to the surface, and to the assignment of the excess electronic state as a nonbonding Ti state.

Figure 3 also evidences a global shift of the bands ($\simeq +0.7$ eV) towards higher energies, together with a band narrowing, upon adsorption. The VB narrowing is of the order of 0.4 eV. It compares well with the photoemission results[13] and suggests an increase of ionicity in the substrate. The narrowing is much larger for the Ti_{3s} and Ti_{3p} bands (Fig. 4), which indicates inhomogeneous shifts in the substrate, with the Ti states of lowest energies experiencing the largest shifts.

The Bader's charge analysis gives low electron numbers and thus large ionic charges on the Na atoms ($+0.91$ and $+0.90$ in the *A* and *B* configurations, respectively), consistently with the nature of the excess electronic state. The Na atoms are thus nearly fully ionized and transfer their valence electron to the TiO_2 substrate. In the substrate, an accumulation of electrons takes place in the vicinity of the adsorbed Na, of the order of 0.4 electron within a distance of 5.5 a.u. It is mainly localized on the bridging oxygens and the sixfold coordinated surface Ti atoms. The formal charge of the titanium atoms on which the excess electronic state is localized, on the other hand, changes by less than $0.06e$. This number is much smaller than the value of $0.25e$ that would be expected if the two electrons of the excess states were equally shared between these eight Ti atoms in the supercell. This apparent contradiction results from the existence of screening effects that wash out a part of the perturbation: the self-consistent variation of electron density upon adsorption indeed results from (i) the density of the excess electronic state, which, in the present case, corresponds to a donation of about one electron per Na atom to the substrate and (ii) the response of the substrate electrons to the electrostatic perturbation represented by the Na cation plus the donated electron (screening effects). A more comprehensive discussion of screening is provided in the next section.

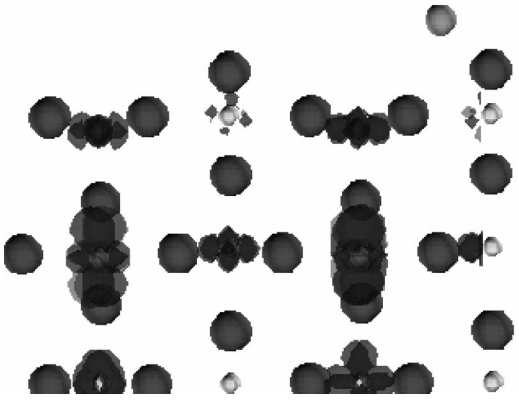

FIG. 4. Isodensity surface of the excess electronic state of $Na/TiO_2(110)$ at $c=1/8$ ML in the *A* geometry, at $\approx 4\%$ of the maximum density. Ti, Na, and O atoms are shown as small light gray balls, medium gray balls, and large dark gray balls, respectively.

C. Discussion

The present calculation predicts the adsorption site of lowest energy to be the *A* site for a Na concentration of $c=1/8$ ML and the corresponding adsorption energy to be equal to $E_{ads}=2.42$ eV. The energy ordering of the two competing *A* and *B* adsorption configurations can be explained on the basis of classical arguments correlating the bond lengths with the bond strengths (i.e., the shorter the bond, the larger the binding energy). Thus, the LDA seems to provide the correct ordering though the difference between *A* and *B* configuration energies may be quantitatively affected by the actual treatment of exchange and correlation effects. These results can be compared to experimental data[41] and theoretical predictions[20] performed in the limit of very small coverage.

From the experimental point of view, an ion-diffraction measurement concludes that the *B* site is preferred,[41] at variance with our results. The discrepancy may be due to the finite Na coverage present in our simulation—note that the energy difference between *A* and *B* sites that we find is not large and may possibly be overcome by changing the Na concentration. However, it should also be noted that ion-diffraction experiments sometimes give results that differ from those obtained with other structural techniques, e.g., GIXD (grazing incidence x-ray diffraction). This is the case for the determination of the relaxation of the clean $TiO_2(110)$ surface.[42,43]

From the theoretical point of view, embedded cluster calculations predict Na adsorption in an *A* site,[20] but with a very elongated Na-O^P bond length and with an energy equal to 7.11 eV. At variance with simulations in which adsorbates are periodically repeated, only one Na atom is effectively present in the calculation of Ref. 20. As regards the value of E_{ads}, we will see in Sec. IV, that an increase by no more than 0.5 eV can be expected in our calculation if the Na concentration is extrapolated to zero. Finite concentration effects are thus not responsible for the huge discrepancy in E_{ads}, which could rather be assigned to the different treatments of exchange and correlations between DFT-LDA and HF-type calculations. For example, in the embedded cluster HF calculation of $K/TiO_2(110)$, the authors of Ref. 18 evidence an almost complete localization of the excess spin on a single Ti—one surface fivefold coordinated Ti—leading to an energy stabilization of nearly 3 eV. Such spin localization is effectively not found in our DFT-LDA study.

As regards the adsorption geometry, we find that the Na-O^P bond length is significantly larger than the Na-O^B one (4.53 a.u. vs 4.25 a.u.) but not as much as in the embedded cluster study (6.39 a.u. vs 4.46 a.u.). Extrapolation to zero concentration, based on Sec. IV results, suggests that the difference between d_{Na-O^P} and d_{Na-O^B} indeed increases at lower concentrations. This trend is also obeyed in the HF embedded cluster calculation of Ref. 21, which compares the adsorption of one and two Na atoms on a TiO_2 cluster and finds $d_{Na-O^P}-d_{Na-O^B}$ equal to 1.93 a.u. in the former case and 0.77 a.u. in the latter. However, we would not expect extrapolation to zero concentration in our calculation to lead to a nearly total bond disruption as in Ref. 20.

The localization of the excess electronic state that we find on some titanium atoms of the substrate subsurface layer appears to be at variance with the widespread opinion that the electron transfer should take place towards the less coordinated Ti, i.e., the fivefold surface Ti. In order to disentangle the respective roles of the adsorbates and substrate in this localization, we have performed a separate study of a clean $TiO_2(110)$ surface with one excess electron per 2D supercell. The resulting excess state wave function was found to be nearly indistinguishable from that represented in Fig. 4. This indicates that the localization of the excess states is largely influenced by the properties of the clean surface and rather insensitive to the presence of the adsorbed Na.

To interpret more quantitatively this observation, and make a link with a previous study of titanium-oxide clusters,[30] in which we had shown that the localization of the excess states, of nonbonding Ti character, is driven by the inhomogeneities of the electrostatic potential *V*, we have estimated the values of *V* acting on the different titanium atoms, under the assumption of uniform ionic point charges in the substrate obeying the neutrality condition $Q_{Ti}+2Q_O=0$. In the relaxed geometry, we indeed find that, in absolute value, *V* is minimum on those Ti atoms on which the excess state localizes, while on the bulk-truncated substrate in which no relaxation is allowed, the surface fivefold coordinated Ti experience the smallest *V*. We thus come to the conclusion that the localization of the excess state obeys the same rule as in clusters, and that relaxation effects are responsible for the fact that the site with the lowest coordination number (fivefold coordinated surface Ti) no longer coincides with the site experiencing the lowest electrostatic potential.

The electron-density redistribution induced by adsorption (by the presence of Na^+ and the filling of an excess state) can be described following a scheme based on ionocovalent screening that was presented in an earlier work.[30] For a perturbation localized on a single site, the mechanism of screening consists of ionicity enhancements and reductions that alternate along the bonds away from the perturbing charge, thus allowing a net flow of electron density. Bond-length variations result, with dilations (contractions) when the bond becomes more ionic (covalent).

Here, a filled excess state and a Na cation simultaneously perturb the $TiO_2(110)$ surface, with charges of opposite sign distributed on several sites. They give rise to two electronic screening flows, one away from the subsurface Ti atoms, and the other directed towards the adsorbed sodiums. However, due to the proximity of the two perturbations, the two flows interfere, and we can follow them by simply inspecting the variation of the Ti-O bond lengths. At the subsurface Ti on which the excess state is localized, all the Ti-O bond lengths increase, indicating an electron flow away from the site, which washes out a part of the negative perturbing charge. Further away, by following the [110] direction towards the surface, the Ti-O bond lengths are alternatively contracted and elongated by more than 0.1 a.u., indicating an electron transfer towards the bridging oxygens. As a whole, with respect to the clean surface, the total electron number on the subsurface Ti does not increase by more than $0.1|e|$, while on the bridging oxygens it reaches $+0.13|e|$. The increase of ionicity around the perturbing charges is consistent with the slight narrowing of the VB found in the experiment as well as in the calculations.

This scheme helps understanding that the localization of the perturbing charges, and more specifically of the excess electronic state, does not coincide with the actual charge-density redistribution, that is, the difference of the electron densities with and without the perturbation. It also shows that de-relaxation is a fingerprint of screening effects, that takes place through variations of the iono-covalent character of the Ti-O bond.

IV. EVOLUTION OF ADSORPTION PROPERTIES WITH COVERAGE

We now examine the evolution of the adsorption characteristics as a function of the Na coverage *c*, with particular

TABLE II. Adsorption energy E_{ads}, Na-O distances and Na electron number N_{Na} as a function of sodium coverage c ($n=3$ slab calculations). The results discussed in Sec. III, which were obtained with the $n=5$ slab and for $c=1/8$, are recalled in brackets. The last line gives the results of a periodic HF calculation[22] at $c=1/2$ ML.

Coverage	E_{ads} (eV)		d_{Na-O^B} (a.u.)		d_{Na-O^P} (a.u.)		N_{Na}	
1/8 ML	2.91	(2.42)	4.09	(4.25)	4.28	(4.53)	0.09	(0.09)
1/4 ML	2.44		4.12		4.36		0.13	
1/2 ML	2.12		4.39		4.42		0.29	
1/2 ML (Ref. 22)			4.18		4.33			

attention to the onset of covalent interactions among adsorbates. We consider coverages of 1/8, 1/4, and 1/2 ML, with arrangements of sodium in the *A*-configuration, which minimize the electrostatic repulsion between Na^+ ions. The calculations are performed for $n=3$ slabs separated by 10 a.u. of vacuum, within the LDA approximation to describe exchange and correlation effects. As far as the adsorption geometry and the Na electron number are concerned, the results obtained in that way for $c=1/8$ ML compare well with those reported in the preceding section (see Table II), which are valid for $n=5$ slabs. However, the aim of the present section is not to achieve the maximum absolute accuracy on the adsorption energetics, but rather to explore the trend in the energy variations as a function of coverage. Similarly, we will not focus on absolute bond lengths, but rather on their evolution as a function of c.

For the three coverages under consideration, there are 2, 4, and 8 excess electron states with respect to the clean slabs, respectively. To mimic the electron density that would be obtained in a spin-polarized calculation, we constrain their filling factors to be 1,1 for $c=1/8$ ML, 1,1,1,1 for $c=1/4$ ML, and 2,2,1,1,1,1 for $c=1/2$ ML.

A. Results

In Fig. 5 the configurations obtained at the end of the structure optimization are shown. The adsorption energies E_{ads}, Na-O distances and Na electron numbers N_{Na} are reported in Table II.

Adsorption energies monotonically decrease from $c=1/8$ to $c=1/2$ ML, evidencing an effective repulsion between adsorbates. Na-O bond lengths, on the other hand, as well as Na electron numbers increase with coverage. These variations are weak between $c=1/8$ and $c=1/4$ ML but much more significant from $c=1/4$ to $c=1/2$ ML. As far as the nature of the Na adsorption site is concerned, at low coverage ($c\leqslant 1/4$) it can be defined as a bridge adsorption site, consistently with the inequivalent ($\simeq 5\%$) Na-O^B and Na-O^P bond lengths reported in Table II. At $c=1/2$ ML, the latter ones are practically equivalent, indicating a transformation of the adsorption site from bridge to hollow. As a whole, the results of Table II, indicate a general weakening of the ionic character of the interfacial Na-O bonding and a reinforcement of the lateral interaction between adsorbates.

At all coverage, alternatively elongated and contracted Ti-O bonds along the [110] direction are found. They are the

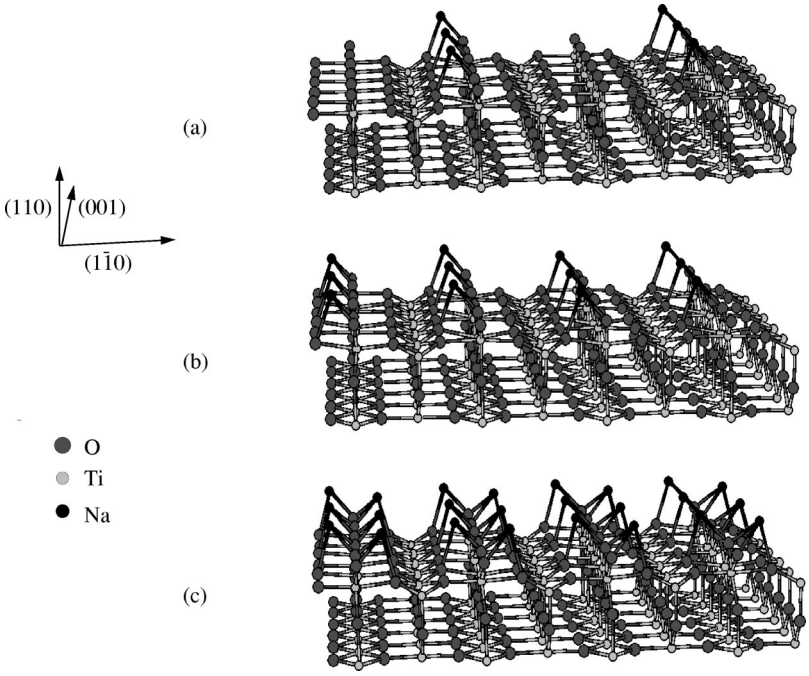

FIG. 5. Adsorption *A* configurations for (a): $c=1/8$ ML, (b): $c=1/4$ ML, and (c): $c=1/2$ ML. Only the upper half parts of the slabs are represented.

TABLE III. Electron number on the Na layer, and variations of electron numbers on the first two TiO_2 layers with respect to the clean surface. The sum of these quantities is equal to N_{excess}, the total number of excess electrons donated by the adsorbed sodiums, which is given in the last column.

Coverage	Na layer	1st TiO_2 layer	2nd TiO_2 layer	N_{excess}
1/8 ML	+0.09	+0.71	+0.20	1
1/4 ML	+0.26	+1.42	+0.32	2
1/2 ML	+1.16	+2.52	+0.32	4

manifestation of screening effects, which can be quantified through variations of the electron density integrated over the different layers, given in Table III. As discussed in Sec. III, these data are consistent with the existence of an electron flux towards the surface plane. This flux affects a single bridging oxygen row per supercell at $c=1/8$ ML (Fig. 3) and all the bridging rows at higher coverage (Fig. 5). Derelaxation occurs in the substrate below the adsorbates.

The DOS in the Ti_{3s}, Ti_{3p}, and VB energy windows are represented in Fig. 6, for the three coverages. The characteristics already noted at $c=1/8$ ML—presence of excess states in the surface gap, shift of the bands towards higher energies, and narrowing of the bands—are present at all coverage, with more pronounced shifts and narrowing as coverage grows up. The excess electron states are found in the energy ranges 2.2–2.3 eV ($c=1/8$ ML), 2.3–2.4 eV ($c=1/4$ ML) and 1.8–2.3 eV ($c=1/2$ ML) above the VB maximum. The absolute positions should be taken only as indicative, because of the small slab thickness used. As shown in Fig. 7, the excess states are mostly Ti-like whatever the coverage c. The higher the coverage, the larger the number of inequivalent Ti in the subsurface layer on which the excess state is localized. Interestingly, at $c=1/2$ ML, the excess state of lowest energy also exhibits some density delocalized on the Na atoms, which is shown in Fig. 8.

B. Discussion

The variations of the adsorption energetics, the localization of the excess state and the screening effects evidence the competition between Na-Na and Na-substrate interactions as the coverage increases. We will discuss these points successively, and compare with the case of K adsorption.

(a) *Adsorption energetics*: In order to get an insight into the dependence of effective Na-Na interactions as a function of coverage c, from the data of Table II, we write the adsorption energy E_{ads} at a given Na coverage, as $E_{ads}(c)=E_{ads}(0)+\Delta E(c)$. $E_{ads}(0)$ is the value of the adsorption

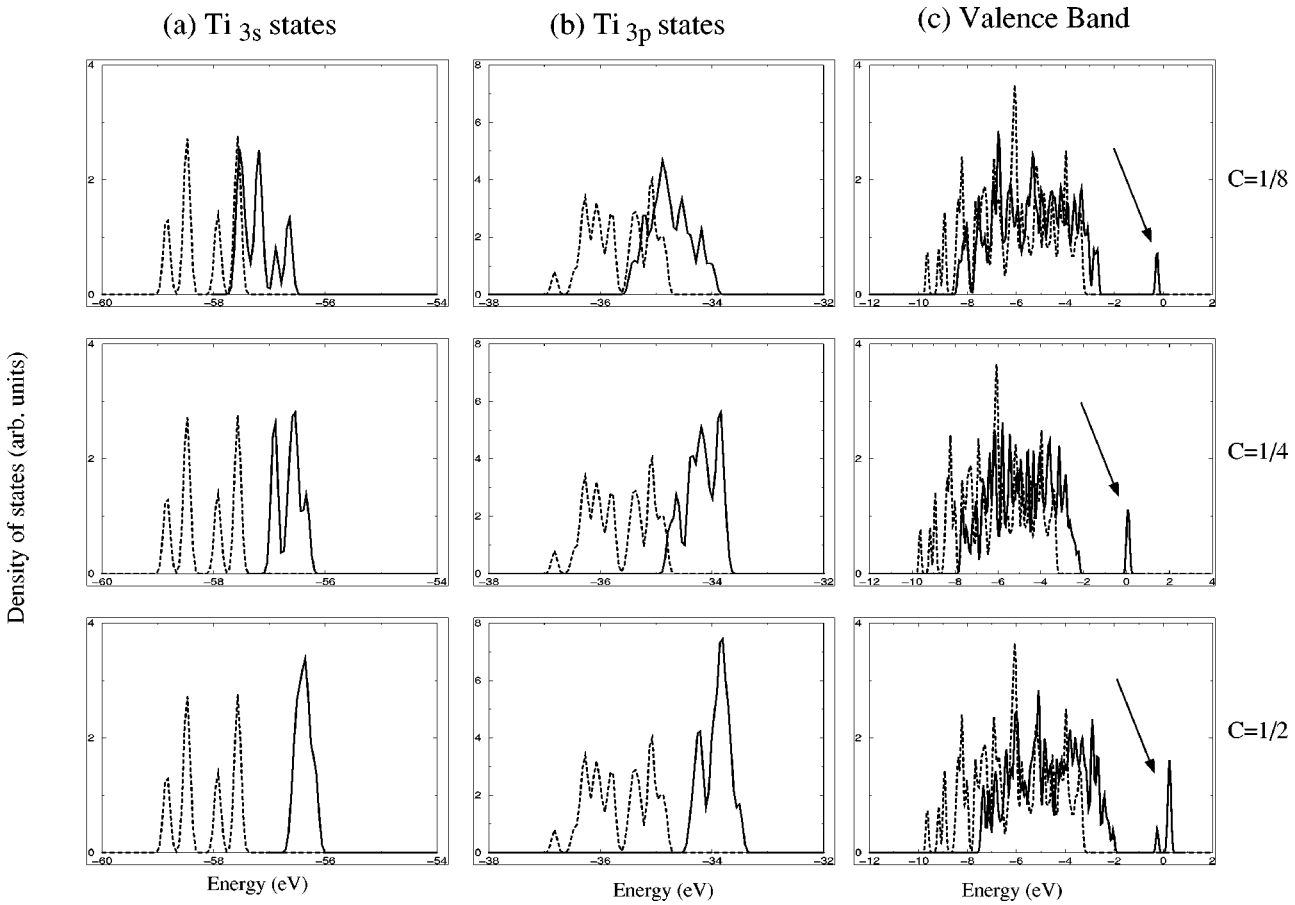

FIG. 6. $Na/TiO_2(110)$ DOS (arbitrary units) as a function of energy (in eV) in (a) the Ti_{3s}, (b): the Ti_{3p}, and (c): the VB energy regions, at three different coverages, $c=1/8$ ML, 1/4 ML, and 1/2 ML. Solid lines: $Na/TiO_2(110)$. Dashed lines: clean $TiO_2(110)$ surface. The arrow points the position of the excess electronic state of the $Na/TiO_2(110)$ surface.

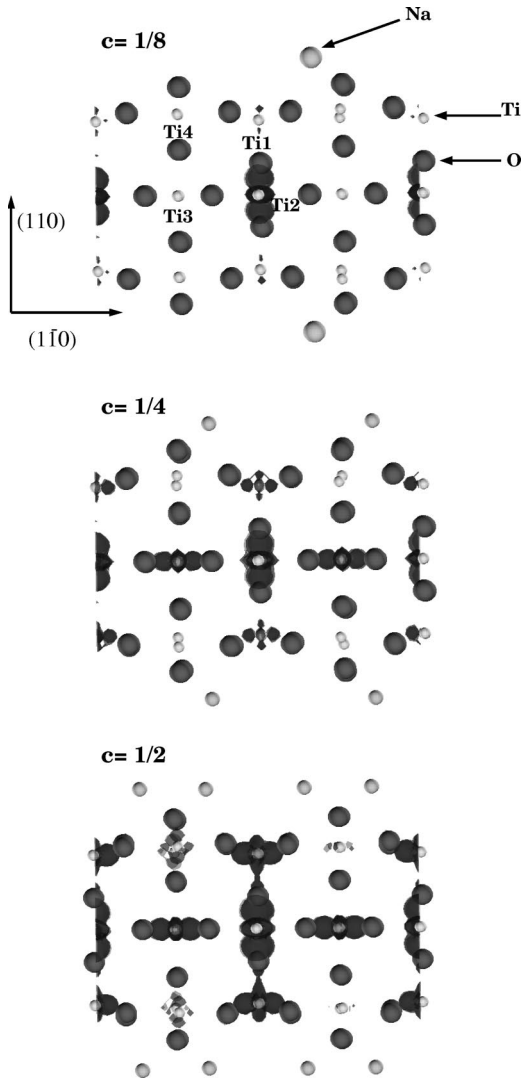

FIG. 7. Isodensity surfaces of the excess-electron states ($\approx 6\%$ of the maximum density) (a): $c=1/8$ ML; (b) $c=1/4$ ML; (c): $c=1/2$ ML.

energy in the limit of zero coverage—isolated atom adsorption—and $\Delta E(c)$ contains the information on adsorbate-adsorbate interactions. We write the latter as a sum of pair terms, varying as an inverse power of the Na-Na distances R_{ij}: $\Delta E(c)=1/2\Sigma_{ij}A/R_{ij}^{n}$. The best fit to our data is obtained for $n=1$, $E_{ads}(0)=3.44$ eV and A positive. As mentioned in Sec. III, the extrapolated value of E_{ads} for zero coverage differs from that obtained at $c=1/8$ ML by only ≈ 0.5 eV. The results at $c=1/8$ ML thus give a good account of the adsorption characteristics of a single Na atom. The positive character of the constant A implies that the adsorbates repel each other in an effective way. The increase of Na-Na repulsion as coverage grows also reflects itself in the adsorption geometry. We find a modification of the adsorption site symmetry, from distorted hollow at low coverage towards symmetric hollow at $c=1/2$ ML, the latter permitting a better screening of the Na-Na direct interaction by the negative charges borne by the bridging oxygens.

(b) *Localization of the excess states and screening effects*: According to Figs. 7 and 8, the excess state localization pre-

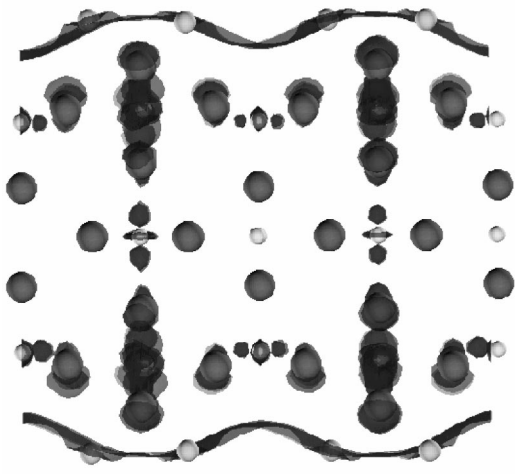

FIG. 8. Isodensity surface of the lowest-energy excess-electron state ($\approx 6\%$ of the maximum density) at $c=1/2$ ML, which evidences some delocalization of the wave function on the adsorbed Na. Ti, Na, and O atoms are shown as small light gray balls, medium gray balls, and large dark gray balls, respectively.

sents two main characteristics as coverage grows. First, the weight of the excess states is distributed over more and more substrate Ti atoms, including subsurface as well as surface sites. In addition, at $c=1/2$ ML, the lowest-energy excess state presents some delocalized character on the Na atoms. This evolution results from a crossing of Ti-like and Na-like levels as c increases. At low coverage, the lowest conduction (CB) state has a nonbonding Ti character and is localized on the subsurface Ti experiencing the smallest Madelung potential (in absolute value), as explained in Sec. III. As c increases, these Ti levels shift towards higher energy, due to the on-site electron-electron repulsion and start crossing levels from other substrate Ti. This crossing results (i) in a change of character of the bottom of the CB that involves a band of d levels arising from inequivalent Ti, and (ii) in a narrowing of the Ti_{3s} or Ti_{3p} DOS, as seen in Fig. 6.

Simultaneously, Na-like energy levels shift towards lower energy, due to (i) the electrostatic potential created by neighboring Na ions, and to (ii) the reduction of Na-Na distances, which promotes bond formation. It is, therefore, expected that a crossing between Na and Ti states occurs for some critical coverage, which should be accompanied by a noticeable increase of the Na electron number N_{Na}. Our results show a minor variation of N_{Na} from $c=1/8$ to $c=1/4$ ML, which means that, in this coverage range, the correct physical picture is that of a system still largely dominated by ionic interaction between the surface and the adsorbates. The accumulation of electrons in the surface layer, reported in Table III is due to screening effects, which increase the ionicity of the Ti-O surface bonds and are concomitant with the narrowing of the VB DOS in Fig. 6.

Increasing the coverage from $c=1/4$ to $c=1/2$ ML, N_{Na} increases significantly, and one excess state acquires some weight on the adsorbed layer, suggesting that Ti and Na states have comparable energies. Our calculations do not allow to give a quantitative estimate of the critical coverage at

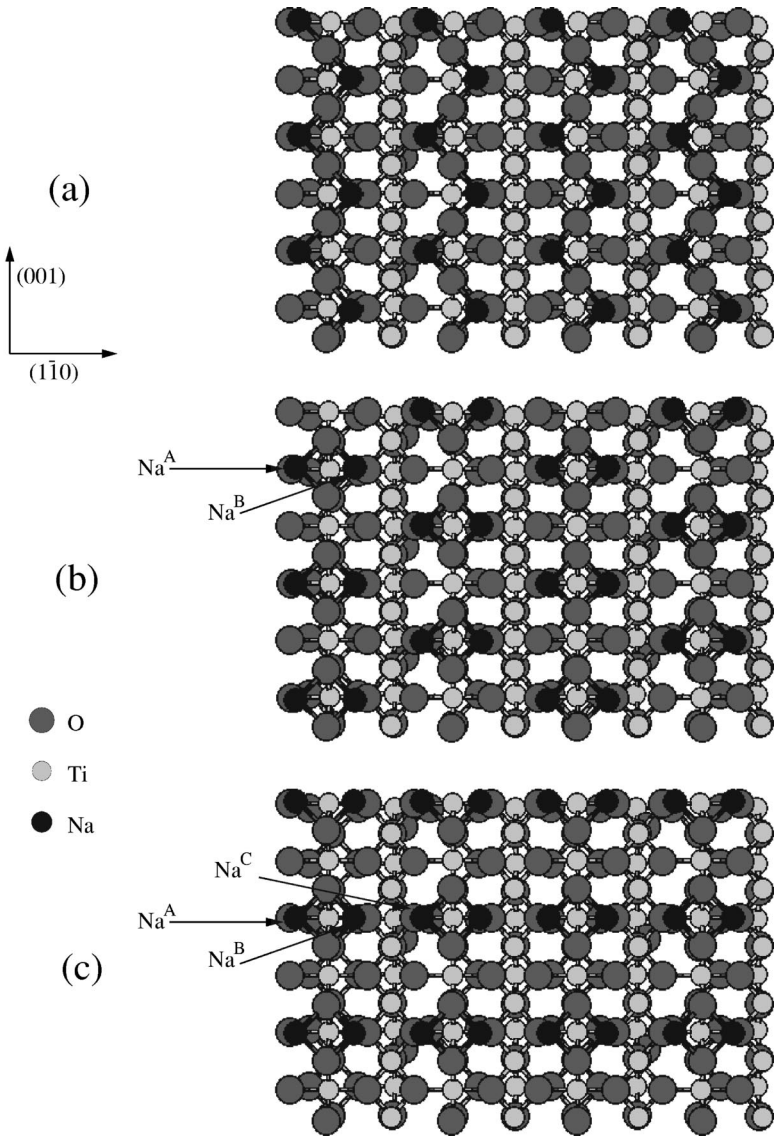

FIG. 9. Three Na configurations at $c = 1/2$ ML.

which metallization of the adsorbate layer takes place. They suggest that the crossover between the two adsorption regimes is rather smooth.

(c) *Comparison between* K *and* Na *adsorption on* $TiO_2(110)$: The trends that we have found in the case of Na adsorption present some similarities with those found in the system $K/TiO_2(110)$. K coverage equal to $c = 1/4$ ML (Ref. 18) and $c = 1/2$ ML (Ref. 19) has been considered and studied by a periodic Hartree-Fock method. In Ref. 18, two configurations $C1$ and $C2$ have been simulated, with large ($d = 5.87$ Å) and short ($d = 4.08$ Å) K-K distances, respectively, the latter being close to that relevant to $c = 1/2$ ML in Ref. 19. The adsorbate-substrate electron transfer was estimated by means of a Mulliken charge analysis. The absolute values of the Mulliken charges Q_K are not comparable to those derived from a Bader-type analysis, but we will only discuss the charge modifications as coverage increase. Q_K is equal to 0.86 at $c = 1/4$ ML for $C1$ and equal to 0.45 and 0.43 at $c = 1/4$ ML for $C2$ and $c = 1/2$ ML, respectively. These results show that K-K interactions drive the value of the adsorbate-substrate charge transfer. The reduction of Q_K between $c = 1/4$ and $c = 1/2$ ML is much stronger than in the case of Na adsorption. This suggests that, at $c = 1/2$ ML, the K levels are shifted towards lower energy than Na levels. The existence of a stronger electrostatic potential due to the other adsorbates can induce such an effect. It would then result from the large size of the K atoms, making it difficulty to screen K-K interactions. We also note that the large K atom size implies that direct bond formation is more effective and can lead to the formation of a wider and more populated adsorbatelike band.

V. RELATIVE STABILITY OF ADSORBATE CONFIGURATIONS AT $C = 1/2$ ML

In order to get a better understanding of the interaction between adsorbates and shed some light on the conditions under which Na_2O units may form, as proposed in Ref. 12, we have considered three configurations of Na atoms in A sites, at a coverage of $c = 1/2$ ML. The first distribution—(a) in Fig. 9—already discussed in the previous section, maximizes the distance between nearest neighbor Na atoms.

TABLE IV. Adsorption energies E_{ads}, geometries, and Na electron numbers N_{Na} for the three configurations displayed in Fig. 9 at $c=1/2$ ML. The shortest Na-Na distance is given for each of them. In (c), N_{Na} includes the contribution (+0.16 electron) of the pseudoatom located between neighboring Na pairs (see text).

Coverage	E_{ads} (eV)	d_{Na-O^B} (a.u.)	d_{Na-O^P} (a.u.)	d_{Na-Na} (a.u.)	N_{Na}
(a)	2.11	4.40	4.39	7.46	+0.29
(b)	2.11	4.43	4.31	5.76	+0.28
(c)	2.09	4.41	4.32	5.59	+0.36

The second distribution (b) involves pairs of Na atoms, on opposite sides of the bridging oxygen rows. The pairs are shifted along the [001] direction from one row to the neighboring one, so that their distance is equal to 10.86 a.u. and 24.35 a.u. along the [001] and the $[1\bar{1}0]$ directions, respectively. In the third distribution (c), Na pairs form rows along $[1\bar{1}0]$, separated by 10.86 a.u. in the [001] direction. We use here the same computational setting as described in Sec. IV. In the search for the ground-state optimized structure, atoms are first located at hollow site positions, small random displacements are then added and relaxation is finally allowed. Actually, only metastable geometries close to the starting configurations are obtained.

Our computed values for the adsorption energies, Na-O bond lengths, shortest Na-Na distances, and Na electron numbers are reported in Table IV. For the three configurations considered, we have found no large Na displacement pattern that can significantly lower the total energy of the system. The three adsorption energies are thus nearly degenerate. The same result can be found using the electrostatic model for Na-Na interaction presented in the previous section. This shows that the long-range interactions of the charged Na ions are more important than their precise positioning within the unit cell.

From a geometrical point of view, the adsorption site is nearly perfectly hollow in the (a) configuration, while, in configurations (b) and (c), d_{Na-O^B} and d_{Na-O^P} differ by about 0.1 a.u. The inequivalent Na-O bonds result from an upward displacement of the two bridging oxygens bound to the Na pair, which allows to screen the Na-Na repulsion. The shortest Na-Na distance is much smaller in (b) and (c) than in (a) (5.76, 5.59, and 7.46 a.u., respectively). In (b), it corresponds to the distance between two atoms belonging to the same pair (labeled Na^A and Na^B in Fig. 9), while in (c) it links atoms belonging to two neighboring pairs (atoms labeled Na^B and Na^C, for example). This difference reflects itself in the topology of the charge density map, which displays a nonnuclear attractor between closest Na atoms in configuration (c). Such pseudoatoms are the fingerprints of covalent interactions. The Na electron number, given in Table IV, includes their contribution, which is shared between the two neighboring Na.

In the geometries that we have considered, it is noteworthy that no pseudoatom exists in between a Na pair, neither in (b) nor in (c). The geometry of the pairs that we have simulated is not exactly equivalent to that of the Na_2O units proposed in Ref. 12 to interpret the $TiO_2(110)$ (4×2) reconstruction induced by Na deposition at $c=1/2$ ML. In this model, four sodiums are adsorbed on the four *A* sites surrounding a single O^B, and, as discussed by Nerlov *et al.*,[13] the stability of these units requires a small Na charge and a large Na-Na covalent bonding. Our results do not point towards a preferred stabilization of these units, whose adsorption energy is expected to be similar to those of the other sodium arrangements considered in our work. In addition, the quasidegeneracy of the various Na arrangements that we have found suggests the possibility of a relatively strong surface disorder at ambient temperature, which may explain why the (4×2) reconstruction was not observed in other experimental studies.[13]

VI. CONCLUSIONS

We have presented a detailed description of sodium adsorption on $TiO_2(110)$ based on DFT-LSDA calculations and charge analysis, up to a half monolayer coverage.

At low Na concentration, we find that the adsorbed sodium atoms are nearly fully ionized and that the excess electron state, at an energy in the surface gap, has a nonbonding diffuse titanium character. Important electron redistributions take place in order to screen the electrostatic perturbation. They induce bond length variations, which are consistent with a surface derelaxation, and a concomitant bandwidth reduction in the valence and Ti_{3s} and Ti_{3p} DOS.

As screening is rather effective in TiO_2, the electron-density difference (with and without the adsorbed Na) shows noticeable discrepancies with the distribution of the excess state. The effective charge of adsorbed Na atoms decreases slowly in the range $1/8<c<1/2$, while the Na-$TiO_2(110)$ interaction remains mainly ionic in character. The adsorbate-adsorbate interaction can be accurately described by a simple electrostatic model of interaction between effective charges at the coverage considered here. However, an analysis of Na-induced excess states at $c=1/2$ ML shows that the onset of covalent interactions between Na has already occurred at this coverage. At $c=1/2$ ML, we find that adsorption energies are practically insensitive to the details of the Na atom distribution among the low-energy adsorption sites.

ACKNOWLEDGMENTS

The calculations were performed on the the massively parallel CRAY-SGI platforms of the IDRIS/CNRS center in Orsay (France), using the LAUTREC code,[44] under Project No. 004089.

*Corresponding author. Present address: Dipartimento di Ingegneria dei Materiali, Università di Trieste, via A. Valerio 2, 34127 Trieste, Italy. Email: tristan@dimca20.univ.trieste.it

[1] A. Fujishima and K. Honda, Nature (London) **238**, 37 (1972).
[2] J. M. Hermann, Catal. Today **53**, 115 (1998).
[3] M. H. Xu, N. P. Huang, Z. D. Xiao, and Z. H. Lu, Supramol. Sci. **5**, 449 (1998).
[4] U. Diebold, in *Preparation and Treatment for Surface Characterization*, edited by A. W. Czanderna, C. J. Powell, and T. E. Madey (Plenum, New York, 1998).
[5] H. Onishi and Y. Iwasawa, Surf. Sci. **313**, L783 (1994).
[6] U. Diebold, J. P. Pan, and T. E. Madey, Surf. Sci. **331-333**, 845 (1995).
[7] F. Cosandey and T. E. Madey, Surf. Rev. Lett. (to be published).
[8] A. W. Grant and C. T. Campbell, Phys. Rev. B **55**, 1844 (1997).
[9] M. Brause, S. Skordas, and V. Kempter, Surf. Sci. **445**, 224 (2000).
[10] K. Prabhakaran, D. Purdie, R. Casanova, C. A. Muryn, P. J. Hardman, P. L. Wincott, and G. Thornton, Phys. Rev. B **45**, 6969 (1992).
[11] R. Heise and R. Courths, Surf. Sci. **331-333**, 1460 (1995).
[12] H. Onishi, T. Aruga, C. Egawa, and Y. Iwasawa, Surf. Sci. **199**, 54 (1988).
[13] J. Nerlov, S. V. Christensen, S. Weichel, E. H. Pedersen, and P. J. Møller, Surf. Sci. **371**, 321 (1997).
[14] W. Göpel, J. A. Anderson, D. Frankel, M. Jaehnig, K. Phillips, J. A. Schäfer, and G. Rocker, Surf. Sci. **139**, 333 (1984).
[15] R. Wang, N. Sakai, A. Fujishima, T. Watanabe, and K. Hashimoto, J. Phys. Chem. B **103**, 2188 (1999).
[16] R. Souda, W. Hayami, T. Aizawa, and Y. Ishizawa, Surf. Sci. **285**, 265 (1993).
[17] J. Muscat, N. M. Harrison, and G. Thornton, Phys. Rev. B **59**, 15 457 (1999).
[18] T. Bredow, E. Aprà, M. Catti, and G. Pacchioni, Surf. Sci. **418**, 150 (1998).
[19] C. J. Calzado, M. A. San Miguel, and J. F. Sanz, J. Phys. Chem. B **103**, 480 (1999).
[20] M. A. San Miguel, C. J. Calzado, and J. F. Sanz, Int. J. Quantum Chem. **70**, 351 (1998).
[21] M. A. San Miguel, C. J. Calzado, and J. F. Sanz, Surf. Sci. **409**, 92 (1998).
[22] J. F. Sanz and C. M. Zicovich-Wilson, Chem. Phys. Lett. **303**, 111 (1999).
[23] R. F. W. Bader, *Atoms in Molecules—A Quantum Theory* (Oxford University Press, Oxford, 1990).
[24] R. F. W. Bader, Chem. Rev. **91**, 983 (1991).
[25] R. G. Parr and W. Yang, *Density Functional Theory of Atoms and Molecules* (Oxford University Press, New York, 1989).
[26] R. O. Jones and O. Gunnarsson, Rev. Mod. Phys. **61**, 689 (1989).
[27] J. P. Perdew and A. Zunger, Phys. Rev. B **23**, 5048 (1981).
[28] N. Trouiller and J. L. Martins, Phys. Rev. B **43**, 1993 (1991).
[29] L. Kleinman and D. M. Bylander, Phys. Rev. Lett. **48**, 1425 (1982).
[30] T. Albaret, F. Finocchi, and C. Noguera, Faraday Discuss. **114**, 285 (1999).
[31] C. W. Bauschlicher, P. S. Bagus, and C. J. Nelin, Chem. Phys. Lett. **101**, 229 (1983).
[32] S. D. Elliott and R. Ahlrichs, J. Chem. Phys. **109**, 4267 (1998).
[33] T. Albaret, F. Finocchi, and C. Noguera, J. Chem. Phys. **113**, 2238 (2000).
[34] M. Ramamoorthy, D. Vanderbilt, and R. D. King-Smith, Phys. Rev. B **49**, 16 721 (1994).
[35] M. Steinberg and K. Schofield, J. Chem. Phys. **94**, 3901 (1991).
[36] *Crystal Data*, edited by J. D. H. Donnay (William & Heintz, Washington, 1963); *Handbook of Chemistry and Physics*, 72nd ed., edited by D. Lide (CRC Press, Boston, 1992).
[37] J. Akimoto and H. Takei, J. Solid State Chem. **83**, 132 (1989).
[38] Coordination is an ill-defined concept in a noncrystalline or low-dimensional material, in which interatomic distances can exist in a continuous range of values. However, the pair-correlation function usually has its first two peaks reasonably well separated. This allows to define a cut-off distance d_{cut} below which two atoms may be considered as first neighbors, and an average coordination that is the integrated value of the pair-correlation function up to d_{cut}.
[39] C. Noguera, *Physics and Chemistry at Oxide Surfaces* (Cambridge University Press, Cambridge, 1996).
[40] J. Nerlov, Q. Ge, and P. J. Møller, Surf. Sci. **348**, 28 (1996).
[41] B. Hird and R. A. Armstrong, Surf. Sci. Lett. **431**, L570 (1999).
[42] B. Hird and R. A. Armstrong, Surf. Sci. Lett. **385**, L1023 (1997).
[43] E. Asari, T. Suzuki, H. Kawanowa, J. Ahn, W. Hayami, T. Aizawa, and R. Souda, Phys. Rev. B **61**, 5679 (2000).
[44] A. De Vita, A. Canning, and R. Car, EPFL Supercomputing **6**, 22 (1994).